Chemical Engineering Journal 368 (2019) 504–512

Contents lists available at ScienceDirect

Chemical Engineering Journal

journal homepage: www.elsevier.com/locate/cej

On the high performance of a core-shell structured CaO-CuO/MgO@Al_2O_3 material in calcium looping integrated with chemical looping combustion (CaL-CLC)

Jinchen Ma[a,1], Daofeng Mei[b,1], Weiwei Peng[a,1], Xin Tian[a], Danyan Ren[a], Haibo Zhao[a,*]

[a] State Key Laboratory of Coal Combustion, Huazhong University of Science and Technology, Wuhan 430074, PR China
[b] Key Laboratory of Agricultural Equipment in Mid-lower Yangtze River, Ministry of Agriculture and Rural Affairs, Huazhong Agricultural University, Wuhan 430070, China

HIGHLIGHTS

- A core-shell structured CaO-CuO/MgO@Al_2O_3 material was prepared by SATS technique.
- CO_2 uptake capacity of CCMA was obtained at 0.08 [g CO_2·(g material)$^{-1}$].
- Thermal neutrality of CCMA is achieved due to the unique core-shell structure.

ARTICLE INFO

Keywords:
Calcium looping (CaL)
Chemical looping combustion (CLC)
CO_2 capture
Core-shell structure
Sorbents
Thermal neutrality

ABSTRACT

Calcium looping (CaL) is extensively used in post-combustion capture of CO_2 and sorption-enhanced steam methane reforming because of its advantages of low cost and theoretically high CO_2-capture capacity. Despite this, unstable reactivity of sorbent (CaO) and significant heat requirement for $CaCO_3$ calcination were always encountered in CaL. To address the aforementioned issues, a core-shell structured CaO-CuO/MgO@Al_2O_3 sorbent (CCMA for short) was synthesized via the self-assembly template synthesis (SATS) method, and systematically investigated in terms of carbonation, calcination-reduction and oxidation cycles. In comparison to wet-mixing CaO-CuO material (CC), MgO-supported CaO-CuO (CCM) and Al_2O_3-supported CaO-CuO (CCA), the CCMA performed the highest CO_2 uptake capacity, which was quite stable at around 0.08 [g CO_2·(g material)$^{-1}$] in the 30 cyclic tests. In calcination-reduction stage, CaO in CCMA can be fully recovered by the decomposition of $CaCO_3$, meanwhile the corresponding heat requirement can be compensated by the exothermic reaction between CuO and CH_4, i.e., thermal neutrality can be achieved by using CCMA. The Cu in reduced CCMA can be subsequently oxidized back to CuO in the oxidation stage with a conversion of 97–98%, which is much higher than CC, CCM and CCA. After cycles, no serious sintering was observed for the CCMA and the measured crushing strength (1.4 N) was sufficient for fluidization, which, in combination with its high reactivity, makes this material very promising for CaL-CLC process.

1. Introduction

The greenhouse gas CO_2 emitted during the conversion of fossil fuels has been regarded as a major contributor to global warming [1]. Carbon capture and storage (CCS) technology was suggested as an effective route to reduce the atmospheric CO_2 concentration, of which CO_2 capture was considered as a key step [2,3]. In this context, many researches were devoted to the development of pre-combustion, oxy-fuel combustion, chemical looping combustion and post-combustion processes for CO_2 capture [4,5]. Among them, the post-combustion CO_2 capture involving the independent CO_2 absorption step and separation step is regarded as a straightforward method, due to the convenience to be integrated with the flue gas purification process [6–9]. One promising technology of post-combustion CO_2 capture is Calcium Looping (CaL), which uses a recyclable CaO-based sorbent to continuously remove CO_2 from exhaust gas stream at low cost [10]. CaL was also integrated with steam methane reforming to remove CO_2 as soon as it is formed, consequently enhancing the reforming and water-gas shift

* Corresponding author.
E-mail address: hzhao@mail.hust.edu.cn (H. Zhao).
[1] These authors contribute to this work equally.

https://doi.org/10.1016/j.cej.2019.02.188
Received 4 December 2018; Received in revised form 24 February 2019; Accepted 25 February 2019
Available online 01 March 2019
1385-8947/

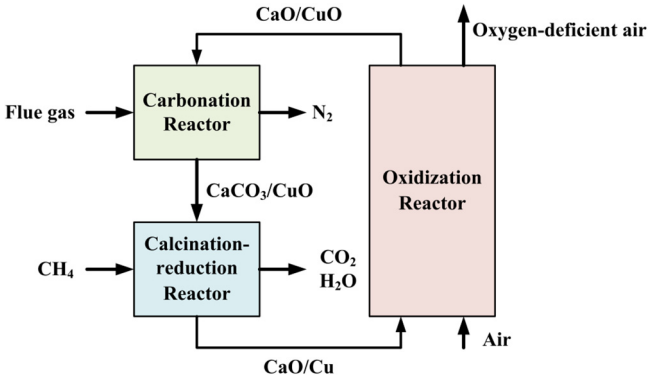

Fig. 1. Schematic description of calcium looping integrated with chemical looping combustion (CaL-CLC) technology.

reactions [6,10]. However, in a conventional CaL, external energy, from oxy-combustion of fuel as an example, must be supplied for the endothermic calcination of $CaCO_3$ during the CaO regeneration process. To reduce the external energy consumption, the CaL was combined with Chemical Looping Combustion (CLC) by Lyon et al. [11], a.k.a CaL-CLC.

In CaL-CLC, combustion of fuel and calcination of $CaCO_3$ take place in the same reactor, where the heat from fuel combustion can be inherently utilized by the endothermic CaO regeneration reaction. A schematic description of CaL-CLC is shown in Fig. 1, where CaO/CuO-based materials are circulated among carbonation, calcination-reduction and oxidation reactors. In the carbonation reactor, CaO absorbs CO_2 in the flue gas stream via the exothermic reaction R(1). The produced CuO/$CaCO_3$ which reserves the heat from reaction R(1) is then moved to the calcination-reduction reactor. There, fuel, e.g. CH_4, is combusted with CuO oxygen carrier via reaction R(2), and releases reaction heat at the calcination-reduction reactor, which at the same time can be used by the calcination of $CaCO_3$ as shown in reaction R(3). The reduced oxygen carrier is then oxidized back to CuO in the oxidation reactor, via reaction R(4), ready to be used in the next cycles. The combination of CaL and CLC in CaL-CLC process has the advantages of avoiding external energy input and inherent CO_2 capture due to the low-penalty separation of CO_2 from H_2O at the outlet of calcination-reduction reactor.

$$CaO + CO_2 = CaCO_3,\ \Delta H^0 = -179kJ/mol \quad (R1)$$

$$4CuO + CH_4 = 4Cu + CO_2 + 2H_2O,\ \Delta H^0 = -178kJ/mol \quad (R2)$$

$$CaCO_3 = CaO + CO_2,\ \Delta H^0 = 179kJ/mol \quad (R3)$$

$$2Cu + O_2 = 2CuO,\ \Delta H^0 = -156kJ/mol \quad (R4)$$

It can be found that the Ca-based sorbent and the oxygen carrier play very important roles in the CaL-CLC. Regarding to the sorbent, various Ca containing materials prepared by different methods were confirmed to be effective in CaL technology [7,12–14]. With respect to the oxygen carrier in CaL-CLC, exothermic properties should be involved in the reaction with fuels. Although various oxygen carriers, including Cu-, Ni-, Co-, Mn- and Fe-based materials, present exothermic behavior in the reaction with CH_4, CO or H_2, the CuO/Cu system exhibits the highest reactivity, oxygen donation capacity, and heat release among these alternative materials [15]. Moreover, using CaO/CuO composite as sorbent/oxygen carrier, process efficiency of CaL-CLC can be improved by around 3% in comparison to CaL, meanwhile more additional power could be obtained in CaL-CLC process [16–17].

In this sense, CaO/CuO-based composites were extensively investigated by various groups [18–25]. Although the feasibility of using CaO/CuO material in CaL-CLC was experimentally confirmed, decay of CO_2 absorption capacity of CaO [18,22–25] and/or the decrease of oxygen donation capacity of CuO [23] are still challenging issues, which lead to unstable performance of these materials under cyclic tests. Therefore, attempts including varying the operation condition [26], thermal pretreatment of sorbents [21], doping foreign ions [19], as well as changing material structures [27], were made to stabilize the reactivity of the CaO/CuO compounds. In the case of varying operation condition and thermal pretreatment, temporary activation of materials can be achieved. However, this was always accompanied by a loss of mechanical stability, that is, particles became fragile after these treatments [26]. The use of nanostructure CaO/CuO in CaL-CLC although can avoid the aforementioned disadvantages, the feasibility of nanoparticles in fluidized bed system has not been experimentally evidenced [21]. In comparison to the aforementioned methods, core-shell structured CuO/CaO can avoid the sintering/agglomeration of core CuO, which assured the stable oxygen donation capacity of the composite material [27]. However, this material exhibited a decrease of CO_2 carrying capacity during cycles [27]. This behavior can be prevented by the doping of Mg^{2+} into the support, despite of the absence of core-shell structure [19]. Consequently, although the recyclability or stability of CaO/CuO-based material is a dominant factor for the further development of CaL-CLC, no systematic method was reported to address this issue yet. In this sense, a CaO/CuO-based material with high mechanical strength, high sintering resistance and stable capacity of CO_2 absorption and oxygen donation during CaL-CLC is lacking.

Taking the advantages of core-shell structure, which had been demonstrated to be more stable reactivity and uniform particle temperature distribution in simulation work [28], and the doping of Mg^{2+}, the present work studied the performance of a core-shell structured CaO-CuO/MgO@Al_2O_3 material (CCMA) which was prepared by a self-assembly template synthesis (SATS) technique developed previously in our group [29–30]. In this material, nano-MgO was covered on the surface of micron-Al_2O_3 via the self-assembly pathway, which successfully inhibited the interaction of CaO/CuO and Al_2O_3. The recyclability/reactivity and physical properties of CCMA were subsequently compared with the non core-shell CaO/CuO, CaO-CuO/Al_2O_3, CaO-CuO/MgO materials, prepared by the same raw materials and comparable mass ratio, by a thermogravimetric analyzer (TGA) under various reacting environments. It was found that stable CO_2 uptake, CaO conversion and oxygen donation capacity were maintained under long-term cyclic tests of carbonation, calcination-reduction and oxidation by using CCMA. This, in combination with good physical properties of CCMA, makes it a very promising candidate to CaL-CLC process.

2. Experimental

2.1. Sample preparation

Four CaO/CuO-based samples, including CaO-CuO/MgO@Al_2O_3 (CCMA), MgO-supported CaO-CuO (CCM), Al_2O_3-supported CaO-CuO (CCA) and wet-mixing CaO-CuO (CC), were prepared, of which the later three samples were prepared and tested for comparison purposes. Similar to our previous work [29], calcium acetate monohydrate [$Ca(CH_3COO)_2{\cdot}H_2O$, Sinopharm Chemical Reagent Co. Ltd., Shanghai, China] and commercial micron alumina powder [Al_2O_3, Sinopharm Chemical Reagent Co., Ltd., Shanghai, China] were used as precursors of CaO and Al_2O_3 support, respectively. Different from our previous work [20], commercial nano-MgO particles [MgO, Aladdin Reagent Co. Ltd., Shanghai, China] were adapted in the present work, which were coated on the surface of micron-Al_2O_3 to prevent the reaction of Al_2O_3 and CaO/CuO. The use of nano-MgO here instead of nano-TiO_2 in the previous work was to further inhibit the interaction of TiO_2 and CaO observed before [29]. Finally, a copper nitrate hydrate [$Cu(NO_3)_2{\cdot}3H_2O$, Sinopharm Chemical Reagent Co. Ltd., Shanghai, China] was selected as the precursor of CuO, which plays the role of oxygen donation between air and fuel. During the preparation of these sorbents, mass ratio of CaO/CuO was maintained at 1:4.9 to avoid its influence on material reactivity, meanwhile to provide equal heat to that

required for $CaCO_3$ decomposition, via the exothermic reaction between CuO and CH_4. In the preparation of CCMA, CCM, and CCA, the mass ratio of all active oxides and supports was kept as (CaO + CuO)/support = 4:1. Furthermore, in the case of CCMA, the mass ratio of MgO to Al_2O_3 supports was MgO/Al_2O_3 = 1:3 to ensure the complete coverage of micron-Al_2O_3 surface by nano-MgO particles. Detailed procedures for the preparation of CCMA, CC, CCM, and CCA are described as follows.

2.1.1. Sample CCMA

The core-shell structured CCMA sorbent was prepared with a well-documented SATS technique developed in our group [29]. Certain amounts of nano-MgO and micron-Al_2O_3 particles, with a mass ratio of MgO/Al_2O_3 = 1:3, were dispersed in 400 mL distilled water heated by a thermostatic bath at 80 °C. The pH value of obtained suspension was then adjusted by titrating a diluted acetic acid or ammonia to pH = 11. After a continuous stirring of 30 min, a mixture of $Ca(CH_3COO)_2{\cdot}H_2O$ and $Cu(NO_3)_2{\cdot}3H_2O$ was introduced under thorough stirring. The compound was then dried at 80 °C for 24 h in an electrically heated oven and subsequently calcined as 950 °C for 2 h to obtain an agglomerate ready for particle preparation.

2.1.2. Sample CC

Calculated masses of $Ca(CH_3COO)_2{\cdot}H_2O$ and $Cu(NO_3)_2{\cdot}3H_2O$ were added into a glass beaker mixed with 400 mL of distilled water at 80 °C in the electrically-heated thermostatic water bath. After stirring for 30 min, the wet precursor was dried at 80 °C for 24 h and then calcined at 950 °C for 2 h both in air atmosphere to form CC agglomerates.

2.1.3. Samples CCM and CCA

Both CCM and CCA were prepared by wet impregnation method as introduced in our previous work [29]. The amounts of $Ca(CH_3COO)_2{\cdot}H_2O$, $Cu(NO_3)_2{\cdot}3H_2O$ and nano-MgO or micron-Al_2O_3 were kept to the mass ratio of (CaO + CuO)/support = 1:4 as introduced above. Nano-MgO or micron-Al_2O_3 particles were fully stirred in a beaker containing 400 mL distilled water for 30 min at 80 °C in thermostatic bath. Subsequently, the mixture of $Ca(CH_3COO)_2{\cdot}H_2O$ and $Cu(NO_3)_2{\cdot}3H_2O$ was added into the beaker under thorough stirring for another 30 min. The net precursor was then dried in an oven at 80 °C for 24 h, and then calcined at 950 °C for 2 h in air atmosphere. The obtained agglomerates were then ready to be crushed for the preparation of CCM and CCA particles.

The above agglomerates of CCMA, CC, CCM, and CCA were crushed, ground and screened. The particles with a size range of 100–300 μm were used in the TGA and characterization tests.

2.2. Cyclic TGA tests

Performances of CCMA, CC, CCM, and CCA materials during carbonation, calcination-reduction and oxidation were tested in a TGA apparatus [WCT-1D, Beijing Optical Instrument Factory, China] which can simultaneously measure the weight change as well as the heat flow in the aforementioned reactions. Prior to cyclic experiments, a preliminary temperature programmed adsorption (TPA) test was performed within the temperature of 500–800 °C in an atmosphere of 15 vol% CO_2 balanced by N_2, which is consistent with the flue gas of conventional boiler, *i.e.* 10–20 vol% CO_2. A significant weight gain was observed when the temperature was close to 750 °C, however, this became negligible for temperatures much higher than 750 °C during the TPA test, mainly due to the thermodynamics property of $CaCO_3$ under 15 vol% CO_2, which is a typical CO_2 concentration from a commercial boiler. In this sense, the temperature of 750 °C was selected as the operation temperature in cyclic tests.

The experimental process was schematically demonstrated in Fig. 2, where a temperature programmed decomposition (TPD) in N_2 for calcination was initiated to reach the isothermal condition at 750 °C. Following the TPD and 30 min of maintaining in 100 vol% N_2, carbonation of the material was carried out in 15 vol% CO_2 with a duration of 10 min, which was followed by a further 8 min of calcination-reduction in 15 vol% CH_4. After that, a flow of 100 vol% N_2 was introduced for 2 min of purge. Finally, the reduced material was oxidized by 100 vol% Air for 10 min. The mass of each sample was around 17.5 mg and the volumetric flow was kept as 60 mL/min to minimize the external film mass transfer and/or inter-particle diffusion according to our previous works [31–32]. The same carbonation, calcination-reduction and oxidation procedure was repeated for 30 times for each material of CCMA, CC, CCM and CCA.

2.3. Characterization

Phase composition of fresh and used CCMA, CC, CCM, and CCA was determined by an X-ray diffraction apparatus [X'pert PRO, PANalytical B.V., Netherlands] using Cu Kα radiation (λ = 0.1542 nm) under 2θ = 10–90°, accelerating voltage of 40 kV and tube current of 40 mA. To evaluate the microstructure of all samples, morphological analysis was performed for both fresh and used samples, using a field emission scanning electron microscope (FSEM) apparatus [FEI Sirion200, Netherlands], shown in *section 4.4.1*. Meanwhile, element distribution of the used CCMA was acquired for analysis using an X-ray energy dispersive spectrometer (EDS) unit [Apollo XLT SDD, Netherlands] equipped with the FSEM, shown in Section 4.4.1. Crushing strength of fresh and used particles with the size of 100–300 μm was determined using a digital dynamometer [FGJ-5, Shimpo, Japan]. The average value of 40 randomly selected particles was taken as the crushing strength of the samples, shown in Section 4.4.2. As shown in Table 1, XRD results indicated that the fresh calcined CCMA was composed of CuO, Ca_2CuO_3, MgO and, Al_2O_3, where the appearance of Ca_2CuO_3 was attributable to the interaction of CaO with the excessive CuO, and this was also detected in the fresh CC with the same CaO/CuO ratio. It should be noted that the Ca_2CuO_3 compound is active in CaL-CLC [21]. As expected, MgO was observed as an individual phase from CuO and Ca_2CuO_3, which suggested the MgO can be used as an inert support here. For CCA, several complicated compositions were formed, that is, except for the CuO, Ca_2CuO_3, and Al_2O_3 phases, different calcium aluminates $(CaO)_x{\cdot}(Al_2O_3)_y$ were also identified, which demonstrated the solid-solid reaction between CaO and Al_2O_3. In comparison to CCA, this type of solid-solid reaction was completely inhibited in the case of CCMA, mainly ascribed to the formation of nano-MgO shell. For CCMA, the usually observed $CuAl_2O_4$ spinel from the solid-solid reaction between CuO and Al_2O_3 [33–34] was absent, which might suggest that the MgO coated on the surface of Al_2O_3 can prevent this reaction. Crushing strength, as shown in Table 1 for fresh materials, is higher than 1 N for all the samples, which would be feasible for fluidization in fluidized bed systems [35].

3. Data evaluation

The carbonation conversion (X_{Ni}) and CO_2 uptake (Y_{Ni}) as a function of cycle number N_i were used to define the stability of CaO sorbent in the composite during the carbonation process. X_{Ni} was obtained as the mass variation over the mass of sample at the initial point of carbonation during cycle N_i, as seen in Eq. (1). Y_{Ni} is calculated as the moles of CO_2 absorbed by CaO in the composite per stoichiometric moles of CO_2 fixed by one mole of CaO, as shown in Eq. (2).

$$X_{N_i} = \frac{m_{N_{i-1}} - m_{N_i}}{m_{N_i}} \tag{1}$$

$$Y_{N_i} = \frac{m_{N_{i-1}} - m_{N_i}}{m_0 \cdot \phi} \cdot \frac{M_{CaO}}{M_{CO_2}} \tag{2}$$

where $m_{N_{i-1}}$ and m_{N_i} are the masses of completely carbonated and initial samples before carbonation in cycle N_i, respectively; m_0 is the

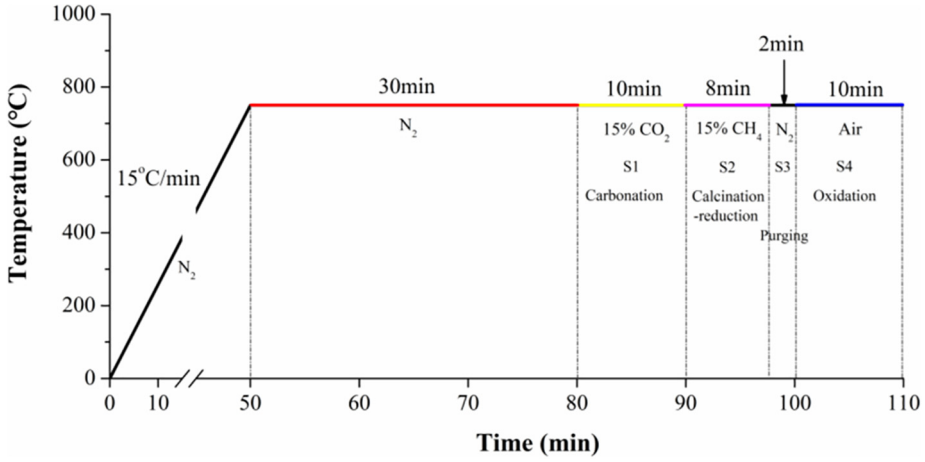

Fig. 2. Experimental setup for TGA tests composed of carbonation, calcination-reduction, and oxidation processes.

original mass of sample and φ is the mass fraction of CaO in m_0. M_{CaO} and M_{CO_2} represent the molar masses of CaO and CO_2, respectively.

The stability of CuO in the CaO/CuO-based compounds was evaluated with the conversion of copper (S_{Ni}) and oxygen donation capacity (T_{Ni}) during oxidation stage of TGA tests. S_{Ni} was determined by the oxygen moles gained over the stoichiometric oxygen moles for fully oxidation of one mole Cu, as seen in Eq. (3), while T_{Ni} was calculated by the mass increment in oxidation stage per mass of fully reduced sample, as seen in Eq. (4).

$$S_{Ni} = \frac{m_{oxy} - m_{red}}{m_0 \cdot \psi} \cdot \frac{M_{Cu}}{M_O} \times 100\% \quad (3)$$

$$T_{Ni} = \frac{m_{oxy} - m_{red}}{m_{red}} \quad (4)$$

where m_{oxy} is the mass of sample after each oxidation step, m_{red} is the mass of sample after full reduction in calcination-reduction step and ψ is the mass fraction of Cu in the original sample. M_{Cu} and M_O are molar masses of Cu and O, respectively.

4. Results and discussion

4.1. Typical cycle in TGA

Fig. 3 shows the normalized mass variations of CCMA, CC, CCM, and CCA samples in the 3rd cycle. As can be seen, an entire cycle is comprised of a carbonation (S1), a calcination-reduction (S2), an inert stage (S3) and an oxidation (S4), corresponding to 10 min in 15 vol% CO_2, 8 min in 15 vol% CH_4, 2 min in 100 vol% N_2 and 10 min in 100 vol % Air, respectively. In step S1, the CaO carbonation reaction happened for all materials, which consisted of a fast reaction stage and a slow reaction stage during the 100 min of carbonation, due to the different reaction mechanisms. In the initial 1.5 min, especially for CCMA, the carbonation was dominated by the chemical reaction control mechanism. However, in the followed 8.5 min, the gas diffusion in product layer became dominant, which resulted in a slow reaction rate. The similar two-step mechanism was also reported elsewhere for the carbonation of CaO [36]. The reaction in step S2 is more complicated,

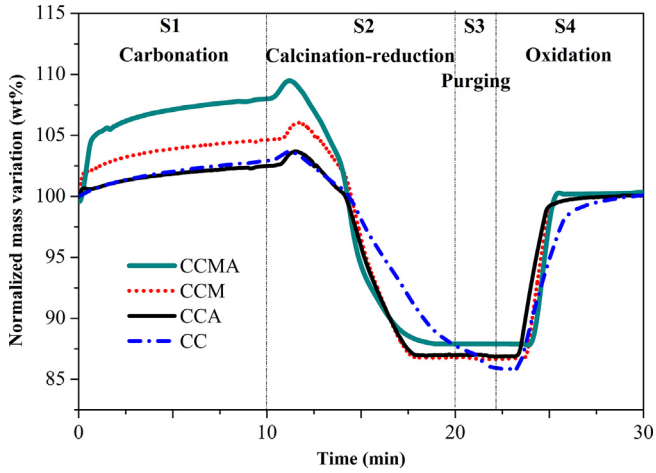

Fig. 3. Normalized mass variation as a function of reaction time for cycle 3 in TGA.

because calcination of previously generated $CaCO_3$ and reduction of CuO by CH_4 occurred simultaneously. A fast weight loss was seen for all the samples, albeit it is difficult to identify the calcination and CuO reduction from the almost linear mass loss in Fig. 3. However, in combination with the heat flow, the two reactions can be distinguished, as will be discussed in the later section. After the rapid weight loss, a stable mass was reached at the end of step S2 for most samples, indicating the calcination-reduction was fully completed. Subsequently, the oxidation step S4 started following 2 min of purge in step S3. It can be observed the Cu generated in S2 was rapidly oxidized to CuO by 100 vol% Air in < 4 min. The plateau of reaction curve in the end of S4 suggested the full oxidation of Cu.

Among the four samples, the doping of Mg and Al elements can improve the CO_2 absorption, excepting the CCA material. In the latter case, although Al_2O_3 was used as a support for CaO/CuO in CCA, a slight lower weight gain than that of CC was observed during the carbonation process. This phenomenon can be attributed to the interaction

Table 1
Composition and crushing strength of fresh and used samples.

XRD phase	CCMA	CC	CCM	CCA
For fresh samples	CuO, Ca_2CuO_3, MgO, Al_2O_3	CuO, Ca_2CuO_3	CuO, Ca_2CuO_3, MgO	CuO, Ca_2CuO_3, Al_2O_3, $CaAl_{12}O_{19}$, $CaAl_2O_4$, $Ca_{12}Al_{14}O_{33}$
For used samples	CuO, CaO, MgO, Al_2O_3	CuO, Ca_2CuO_3, CaO	CuO, Ca_2CuO_3, CaO, MgO	CuO, Ca_2CuO_3, CaO, $Ca_3Al_2O_6$
Crushing strength (N)	1.85 (1.46)[a]	1.58 (1.27)[a]	1.62 (1.27)[a]	1.98 (1.50)[a]

[a] values in brackets are for the used samples.

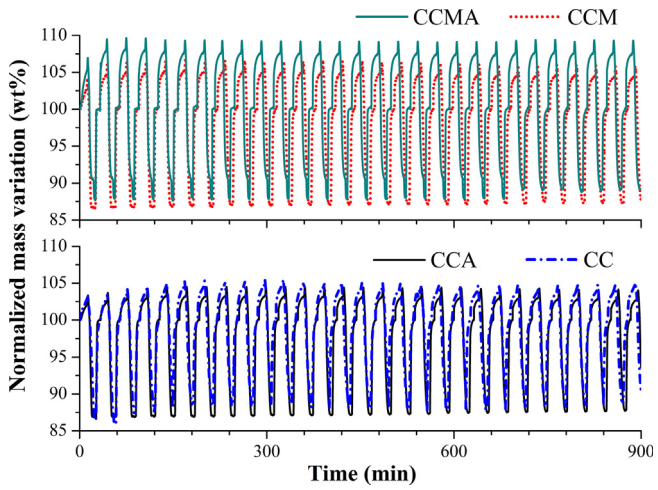

Fig. 4. Normalized mass variation as a function of reaction time during 30 cycles in TGA.

of Al_2O_3 and CaO, which formed aluminates being inactive to carbonation. In comparison to CC and CCA, a considerable increase of CO_2 absorption was found with CCM, mainly due to the stabilization effect of MgO on the reactivity of CaO/CuO [19,25]. Regarding the core-shell structured CCMA, the maximum mass variation can be as high as 108 wt%, which is much higher than that of the other three samples, due to the superiority of the architecture core-shell structure, which demonstrates fully developed uniform pores and high resistance to agglomeration for the active phases (CaO and CuO) after 30 cycles, as mentioned in the XRD result. The difference observed in the followed calcination-reduction and oxidation can be regarded as a result of the different carbonation behaviors.

4.2. Cyclic performance

4.2.1. Carbonation-calcination/reduction-oxidation cycles

Fig. 4 shows the 30 cycles of CCMA, CC, CCM and CCA under the reaction condition, see the details in Section 2.2. During more than 900 min of continuous tests (30 cycles), all samples maintained their feasibility of carbonation, calcination-reduction and oxidation, although some showed deactivation in cycles. The different behaviors observed can be explained by the reasons discussed aforementioned and the physical characteristics shown in the following sections.

4.2.2. Reversibility of CO_2 absorption and release

Fig. 5 describes the CO_2 uptake and carbonation conversion of CCMA, CC, CCM, and CCA as a function of cycle numbers. For all the materials, an increase of CO_2 uptake and carbonation conversion was detected in the initial 1–2 cycles, probably due to the structure change of particles in the reacting environment. In the case of CO_2 uptake in Fig. 5(a), CCA showed a quite low value of 0.03–0.033 [g CO_2·(g material)$^{-1}$] during the 30 cycles, which is only around 28% of the theoretical CO_2 uptake, *i.e.* 0.107 [g CO_2·(g material)$^{-1}$]. The CC exhibited higher CO_2 uptake capacity than CCA during the campaign of tests with a CO_2 uptake in the range of 0.036–0.045 [g CO_2·(g material)$^{-1}$] for CC, which is 27%-34% of the theoretical CO_2 uptake for CC (0.134 [g CO_2·(g material)$^{-1}$]). This was mainly attributed to the interaction of CaO and Al_2O_3 which decreased the available content of CaO in CCA. The CCM sample possessed a higher CO_2 uptake than both CC and CCA in the 30 cycles, which was attributed to the stabilization effect of MgO on the reactivity of CaO/CuO-based materials [19]. Different from the CC, CCM, and CCA samples, the CCMA showed a much higher CO_2 uptake value in the interval of 0.075–0.08 [g CO_2·(g material)$^{-1}$]. More indeed, this CO_2 uptake of CCMA was the most close to the theoretical value, *i.e.* 0.107 [g CO_2·(g material)$^{-1}$], among the four studied samples. In all the materials, CCMA was the most attractive on high and stable CO_2 uptake. In the case of carbonation conversion in Fig. 5(b), similar trend to CO_2 uptake shown in Fig. 5(a) was observed. That is, a considerable decrease of carbonation conversion was encountered for CC, CCM, and CCA during cycles, while CCMA presented the highest and most stable carbonation in all cycles. The results in Fig. 5 suggested that all the studied materials can be reversible in CO_2 uptake and carbonation cycles, while CCMA showed the best performance.

The CO_2 uptake for CCMA was also compared with a previous core-shell $CaO/TiO_2@Al_2O_3$ sorbent developed by our group via SATS technique [29]. During the hundred cycles, the maximum CO_2 uptake of $CaO/TiO_2@Al_2O_3$ was around 0.55 [g CO_2·(g CaO)$^{-1}$], which decreased gradually to 0.53 [g CO_2·(g CaO)$^{-1}$] at cycle 10. However, in the case of core-shell CCMA of the present work, the CO_2 uptake was corresponding to maintain stable at around 0.55 [g CO_2·(g CaO)$^{-1}$] in the 30 cycles. In this sense, a better CO_2 uptake performance of CCMA than CaO/TiO_2-Al_2O_3 can be inferred, which could be ascribed to the inhibition of CaO-Al_2O_3 reaction occurred in CaO-CuO/MgO@Al_2O_3. Moreover, in comparison to $CaO/TiO_2@Al_2O_3$, although CuO was added into CCMA, adverse effects of CuO on the carbonation and CO_2 uptake properties were not observed.

4.2.3. Reversibility of oxygen donation

Relative stable oxygen donation capacity and oxidation conversion of Cu for the CCMA, CC, CCM, and CCA were observed during the 30 cyclic tests, as seen in Fig. 6, which differed from the decrease for CO_2 uptake and carbonation conversion in Fig. 5. This behavior of Cu in the composites was also extensively reported elsewhere [19,22,25,27,37].

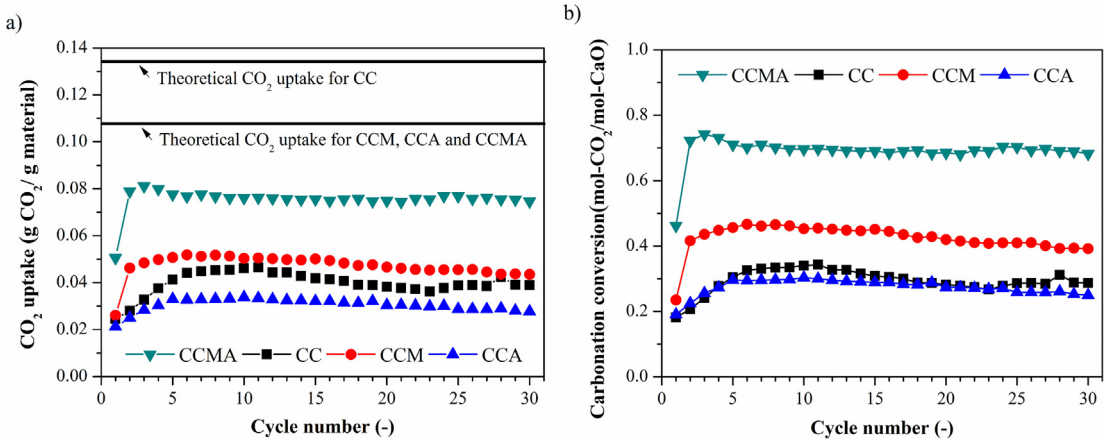

Fig. 5. Variations of (a) CO_2 uptake and (b) carbonation conversion for CCMA, CC, CCM and CCA during the carbonation process of 30 cyclic tests in TGA at 750 °C.

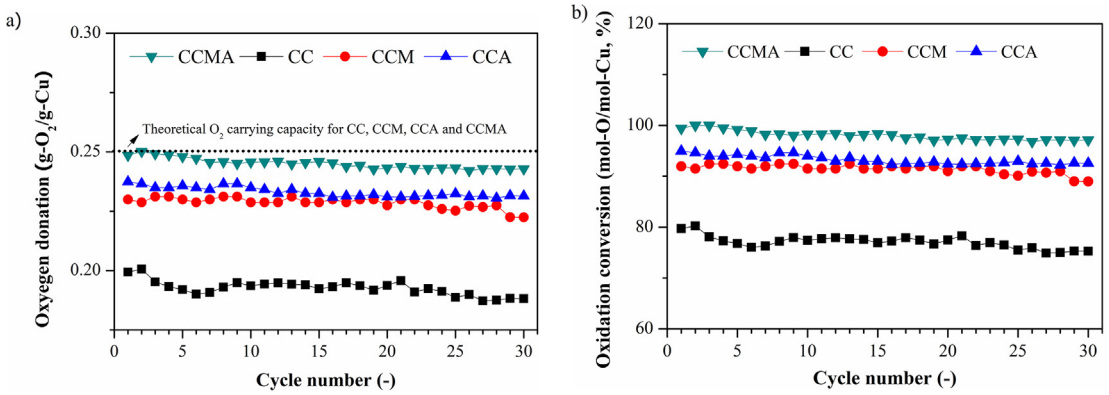

Fig. 6. Variations of (a) oxygen donation capacity and (b) oxidation conversion during 30 cycles in TGA at a temperature of 750 °C.

Despite this, different oxygen donation capacity and oxidation conversion of Cu were noticed among the four samples. The lowest oxygen donation capacity and oxidation conversion of Cu, *i.e.* < 0.20 and < 80%, respectively, were found for CC, although CaO was identified as a support for CuO [27]. This was ascribed to that the CuO content was excessive over CaO in CC (the mass ratio of CuO:CaO was 4.9:1), which resulted in part of free CuO, see Table 1 in the experimental section, showing low reactivity and sintering resistance capacity during cycles [38]. In contrast, the mass fraction of CuO loaded in the other supports MgO, Al_2O_3, and MgO-Al_2O_3 of CCM, CCA and CCMA, respectively, were less than that in CC, however higher oxygen donation capacity and oxidation conversion were obtained for these supports. Among these supports, MgO and Al_2O_3 can result in similar oxygen donation capacity and oxidation conversion as CCM and CCA, owing to the similar CuO loading and the same preparation method. In the case of CCMA, the oxygen donation capacity and oxidation conversion were 10% higher than that of CCM and CCA and 25% higher than that of CC, attributing to the unique characteristics of the core-shell structure of CCMA.

In comparison to a core-shell, cement supported CaO-CuO composite developed by Manovic et al. [27], the CCMA presented a higher oxygen donation capacity, *i.e.* 17 wt% versus 10 wt%. The reason might be the different distribution of elements in the core-shell structure. In the case of Manovic et al. [27], the (CuO + CaO) was prepared as a core which was covered by cement as a shell; however, it was just the opposite for CCMA. The distribution of CuO as a shell in CCMA could facilitate the contact of CuO and fuel gas during calcination-reduction process.

4.3. Thermal neutrality of CCMA

As discussed in Section 2.1, the mass ratio of CaO/CuO = 1:4.9 was designed during the material preparation to reach thermal neutrality of the composite. Here, this feature was checked via the differential thermal analysis (DTA) results during TGA cycles. Fig. 7 showed the DTA signal in typical cycles of CCMA, where the downward and upward peaks, corresponding to the endothermic and exothermal processes, respectively, can be clearly identified. During the carbonation process, an exothermic peak in DTA signal was observed, which corresponded to the chemical reaction control regime, as characterized by a fast mass increase in TGA profile. Following that, no DTA peak can be clearly identified during carbonation, which suggested the weak thermal emission in the diffusion control stage for the reaction between CaO and CO_2. In the calcination-reduction process, a first exothermic upward peak and a second endothermic downward peak were detected, which is because of different reactions occurred there, *i.e.* exothermic CuO reduction by CH_4 and endothermic decomposition of $CaCO_3$. In this case, it can be concluded that the reaction of CuO and CH_4 was dominant in the first period, which was followed by the endothermic

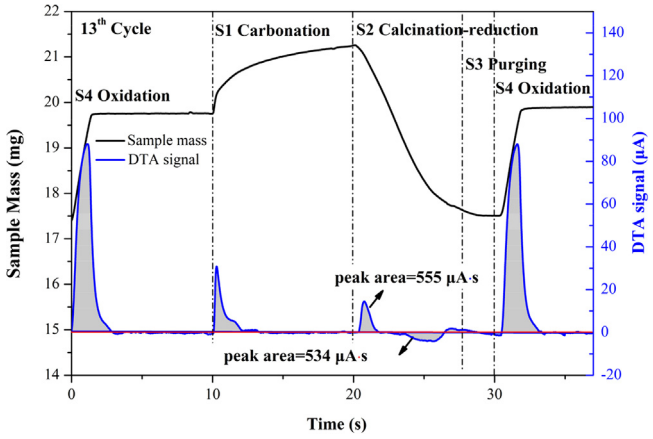

Fig. 7. Variations of sample mass and DTA signal as a function of reaction time during typical cycles composed of carbonation, calcination-reduction and oxidation processes in TGA tests at 750 °C for the CCMA sample.

calcination of $CaCO_3$, dominant to the second period. This is advantageous because the heat required for $CaCO_3$ calcination was ready in advance by the exothermic reaction of CuO and CH_4. The peak areas of the exothermic and endothermic reactions at the 13th cycle were 555 μA·s and 543 μA·s, respectively, calculated by the integration method shown in Fig. 7. More indeed, the heat released is slightly higher than that required for $CaCO_3$ decomposition, which indicated that the heat required for $CaCO_3$ calcination can be totally supplied by the exothermic reaction of CuO and CH_4. In the oxidation, a high upward peak of DTA signal was detected, which was a result of intensive exothermic oxidation of Cu by air.

Moreover, the kinetics of CuO reduction by CH_4 and $CaCO_3$ calcination can be simply discussed according to the specific TG-DTA results. The slope of TG curve corresponding to CLC (*i.e.* $dm/dt \approx 0.65\ mg \cdot min^{-1}$) is somewhat higher than that of calcination process (*i.e.* dm/dt = 0.26–0.65 $mg \cdot min^{-1}$). In this sense, the CLC kinetics is a bit faster than that of calcination under the specific reaction environment, *i.e.* 15 vol% CO_2 + 85 vol% N_2 and 750 °C. However, this cannot be considered as a common kinetics for the comparison of CLC and calcination, because other parameters, such as temperature, gas concentration and particle structure, were not fully considered.

Exothermic and endothermic stability of CCMA was also checked in the 30 cyclic tests, as shown in Fig. 8, where the peaks discussed in Fig. 7 were clearly identified in all cycles. At the same time, stable upward peaks for exothermic reaction and downward peaks for endothermic reaction kept their intensity during 30 cycles. It was found that the difference of the integrated DTA signal between the reduction of CuO and the calcination of $CaCO_3$ was close to zero, especially after the 10th cycle, which indicated the thermal neutrality feature of CCMA.

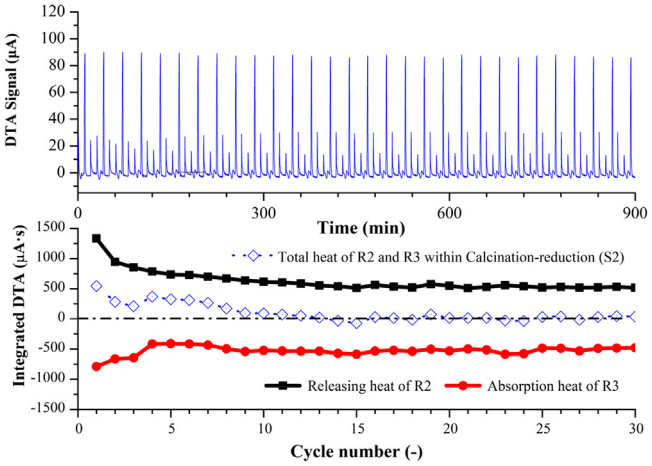

Fig. 8. Variation of DTA signal as a function of reaction time during the 30 cycles composed of carbonation, calcination-reduction and oxidation processes in TGA tests for CCMA at 750 °C.

In addition, stable thermal evolution was observed for CCMA, which further evidenced the stable reactivity of this material, also disscussed in Section 4.2.2 and 4.2.3.

4.4. Physical characterization

4.4.1. Morphology

Microstructures of the fresh and used four samples were compared in Fig. 9. For the fresh samples, porous surface was observed for CCM, CCA and CCMA, whereas smooth and dense surface was found for CC, due to the sintering caused by the absence of proper support materials. This phenomenon confirmed the critical role of proper support materials in the inhibition of sintering and/or agglomeration. The well-developed porous structure of CCM, CCA and CCMA could be considered as a main contributor to the higher carbonation rates of them than CC, as illustrated by the higher initial slopes of carbonation stages in Fig. 3. After 30 cycles, larger grains and fewer pores were found on the surface of CC, CCM and CCA, mainly due to the sintering or "wrapping" observed previously by Qin et al. [22]. Therefore, a decay of CO_2 uptake and carbonation was observed for CC, CCM, and CCA in Fig. 5. On the contrary, the pores of CCMA were better developed during the 30 cycles, which could provide a larger contact area and more active sites for the heterogeneous carbonation reaction. The maintained microstructure of CCMA confirmed again the superiority of core-shell over the other structures involved in this work.

To further confirm the core-shell structure of CCMA, the fresh and cycled particles were cut and analyzed by FSEM-EDS technique. As shown in Fig. 10, a core-shell structure can be clearly identified for the fresh and used CCMA, which was characterized by an Al-rich core and a shell with Mg, Ca and Cu as the main elements. This finding confirmed that the SATS method do derives core-shell structured fresh particles in the present case. The nano-MgO particles were well dispersed on surface of the core micron-Al_2O_3 or formed some clusters to effectively inhibit the interaction between CaO/CuO and the Al_2O_3 support. Meanwhile, the homogenous distribution of active composites CaO and CuO on the external surface can enhance the heterogeneous reactions with CO_2 and CH_4. This was expected during the synthesis of CCMA via SATS technique, where micron-Al_2O_3 in the core was designed as the main framework to support the nano-MgO particles and active components. It was also found that Mg and Ca were both observed in the entire particle, mainly explained by the movement and redistribution of Mg and Ca elements that were usually encountered during the polishing of the mosaic samples used for FSEM-EDS characterization. Despite this, an Al-rich core and a shell with Mg, Ca and Cu elements were both detected for the fresh and used particles, suggesting the stable core-shell structure of CCMA. Meawhile, no siginificant diffusion and/or redisctribution of each element in core and shell was seen. Therefore, the maintenance of core-shell structure of CCMA and stable elements distribution in the 30 cycles make this material a very promising candidate for long-term application in CaL-CLC.

4.4.2. Crushing strength

The crushing strength of fresh and used CCMA, CC, CCM, and CCA listed in Table 1 was further compared in Fig. 11(a) for better evaluation. The fresh calcined materials showed a crushing strength in the interval of 1.58 ± 0.17–1.98 ± 0.15 N in average, higher than the required value for fluidized bed application [35], of which CCA and CCMA have the highest values. In comparison to the fresh materials, some decreases of crushing strength in the range of 19.6–24.2% were detected for the used CC, CCM, CCA and CCMA. Despite this, a crushing strength higher than 1.4 N was found for CCMA after 30 cycles. The variation of crushing strength for CCMA as a function of cycle number was shown in Fig. 11(b). The crushing strength tests for CCMA sample extracted from cycles 1, 5, 10, 20 and 30 suggested that it became stable to ~1.5 N after approximately the 5th cycle. In this case, during the 30 cyclic tests in TGA, the crushing strength of CCMA exhibited an initial decrease, which then became stable in the rest cycles. In this sense, the crushing strength of CCMA should be adequate for the use in fluidization systems [35].

4.5. Economy of CCMA

The economy of the sorbent in CaL-CLC depends on many influencing factors, such as the cost of raw material, the attrition-rate related lifetime and the reaction-kinetics related solids inventory. The

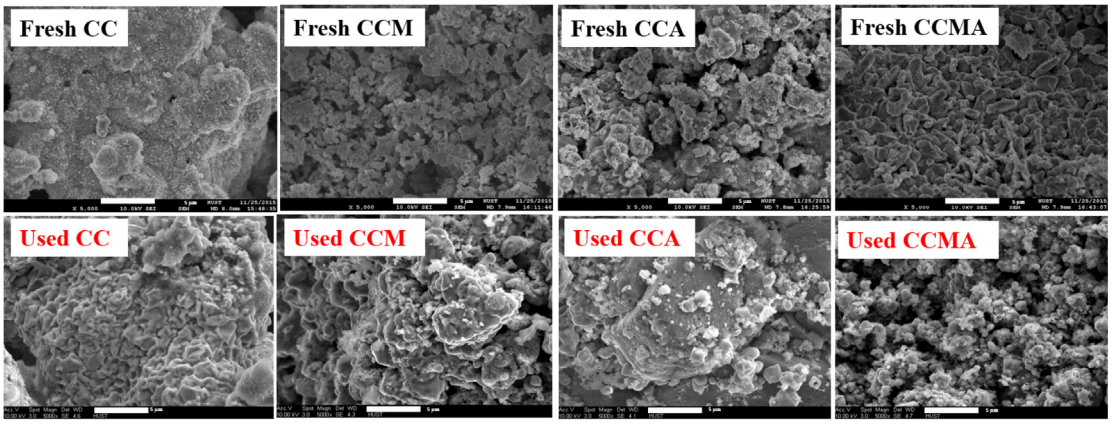

Fig. 9. FSEM images of fresh and used samples (5000 x).

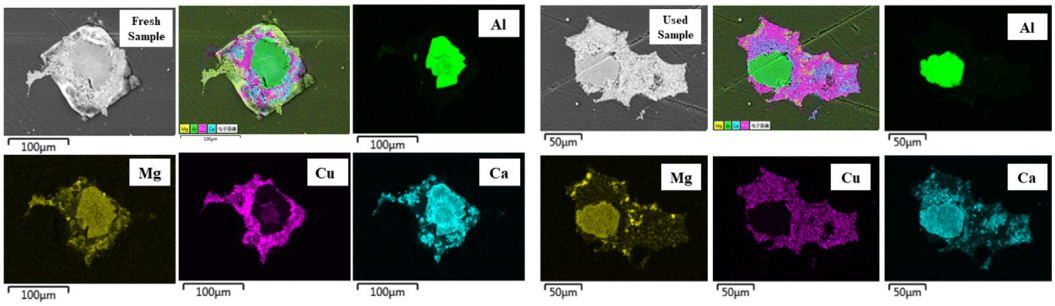

Fig. 10. Microstructure and the distribution of Al, Mg, Ca and Cu elements on the cut cross-section of a particle of the fresh and used CCMA.

determination of the latter two parameters requires long-term tests under fluidization condition and a systematical reaction kinetics study of this material, respectively; however, some of them cannot be accomplished in a micro-reactor, such as the TGA apparatus used in the present work. In this case, the economy of CCMA can only be estimated according to the cost of raw materials, which thus could be simply used for primary comparison purposes.

Regarding the CaL-CLC process, a material denoted as CCM*, containing Ca, Cu and Mg, was extensively investigated by Qin et al. [22]. Although this material was prepared with a wet mixing method, the similar micro-reactor, *i.e.* a TGA apparatus, was also used for characterization. Therefore, the CCM* was used to compare with the CCMA of our present work in terms of their economy depending on the cost of raw material. The unit price of each raw material required for sample preparation was checked according to the industry information website, which is gathered in Table 2. Among the precursors, the costs of nm-MgO and $Cu(CH_3COO)_2{\cdot}H_2O$ are the highest, although the total cost of sample depends highly on their weight percentages.

According to the CO_2 captured by each sample calculated with TGA data, the cost of CCM* and CCMA can be determined. As shown in Fig. 12, the 10th, 20th and 30th cycles of Qin et al. [22] and our tests of CCMA were used as representatives for comparison. It can be seen that the CCM* has a cost of 900–1400 [$·(kg CO_2)$^{-1}$], which was increased as a function of cycle due to the lower CO_2 captured under higher cycle numbers [22]. In comparison to CCM*, the core–shell CCMA showed a much lower cost, being stable at ~180 [$·(kg CO_2)$^{-1}$] in the 30 cycles. It was also noticed that during the preparation of CCM* a much more expensive $Cu(CH_3COO)_2{\cdot}H_2O$ than $Cu(NO_3)_2{\cdot}3H_2O$ for CCMA was used as a precursor. Therefore, to decrease the cost of CCM*, an assumption that the $Cu(NO_3)_2{\cdot}3H_2O$ was used instead of $Cu(CH_3COO)_2{\cdot}H_2O$ to prepare another similar sample CCM**. Despite this, the cost of CCM** could be as high as 460–720 [$·(kg CO_2)$^{-1}$], which is 2.5–4.0 times that of CCMA. It is noted that if the CCMA sorbent can survive 5000 cycles with similar reactivity and attrition resistance at the 30th cycle, the CO_2 capture cost will be ~36 $/t CO_2. As a result, the CCMA material can be considered as a low-cost sorbent during CaL-CLC according to the above estimation. However, it should be emphasized again that the above cost was estimated only according to the cost of raw materials. To get a more accurate cost calculation, the life time and the reaction-kinetics related solids inventory must be determined, but this is out of the scope

Table 2
Unit price of reagents used for sample preparation.

Reagent type	Unit price ($/kg)[a]
μm-Al_2O_3	0.50
nm-MgO	69.69
$Ca(CH_3COO)_2{\cdot}H_2O$	1.50
$Cu(NO_3)_2{\cdot}3H_2O$	4.60
$Cu(CH_3COO)_2{\cdot}H_2O$	20.61

[a] according to information published on www.made-in-china.com and www.aladdin-e.com

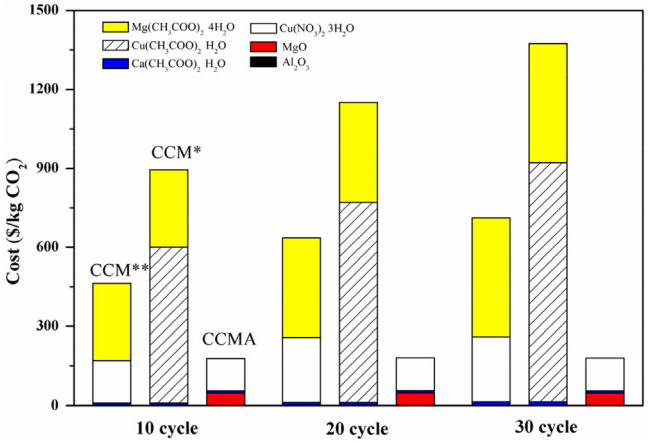

Fig. 12. Cost estimated from raw material price for the 10th, 20th and 30th cycle of CCMA in this work and CCM* in Qin et al. [22], the CCM** is a sample assuming the $Cu(NO_3)_2{\cdot}3H_2O$ was used instead of $Cu(CH_3COO)_2{\cdot}H_2O$ for the preparation of CCM*

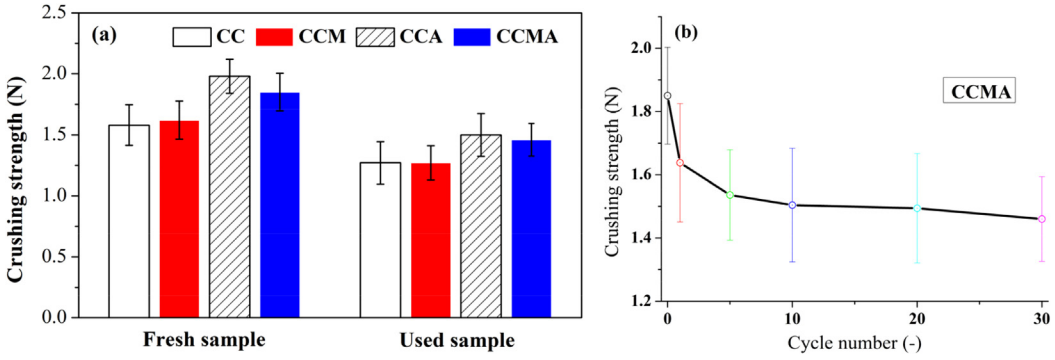

Fig. 11. Crushing strength of (a) the fresh and used CC, CCM, CCA and CCMA samples, (b) the CCMA sample as a function of cycle number.

of the present work.

5. Conclusions

Four materials, *i.e.* core-shell structured CaO-CuO/MgO@Al_2O_3 (CCMA), wet-mixing CaO-CuO (CC), MgO-supported CaO-CuO (CCM) and Al_2O_3-supported CaO-CuO (CCA), were tested to evaluate their performance in calcium looping integrated with chemical looping combustion (CaL-CLC), under the cycles composed of carbonation, calcination-reduction, and oxidation in TGA. Samples of CC, CCM and CCA always suffered from decrease of CO_2 uptake or decay of oxygen donation capacity in the 30 cycles. On the contrary, the CCMA, prepared via the self-assembly template synthesis (SATS) technique and composed of micron-Al_2O_3 core, nano-MgO layer and (CaO + CuO) shell, presented the best reactivity and physical integrity in the cycles. The CO_2 uptake of CCMA in carbonation can be as high as 0.08 [g CO_2·(g material)$^{-1}$] at 750 °C, which is very close to equilibrium value and quite stable in the cycles. Full decomposition of $CaCO_3$ and reduction of CuO in calcination-reduction were accomplished, which suggested the reversibility of the CCMA for CO_2 uptake and release and a stable oxygen donation capacity of around 0.25 [g O_2·(g Cu)$^{-1}$] for CLC process of CaL-CLC. Exothermic reaction of CuO and CH_4 occurred before endothermic decomposition of $CaCO_3$, which is significant for the application in CaL-CLC, because the heat required for calcination has been ready by the CH_4 oxidation. Stable thermal neutrality of CCMA was found during 30 cycles, which is advantageous for economic operation of CaL-CLC due to no external heat requirement. After 30 cycles, the core-shell structure of CCMA was still maintained, where the core micron-Al_2O_3 was completely covered by nano-MgO particles, inhibiting the interaction between CaO/CuO and Al_2O_3. In combination with the stable high crushing strength of ~1.5 N and the stable raw material cost of ~180 [$·(kg CO_2)$^{-1}$], CCMA can be considered as a very promising candidate for CaL-CLC.

Acknowledgements

This work was supported by “National Key R & D Program of China (2016YFB0600801)” and “National Natural Science Foundation of China (51522603)”. Meanwhile, the staff from the Analytical and Testing Center, Huazhong University of Science and Technology, are appreciated for the relevant analytical work.

References

[1] W.P. Gabrielle, D. Hadi, M.D. Tim, R. Isha, Influencing attitudes toward carbon capture and sequestration: a social marketing approach, Environ. Sci. Technol. 45 (2011) 6743–6751.
[2] P. Fontina, T. George, M. Tatiana, Advanced exergoenvironmental analysis of a near-zero emission power plant with chemical looping combustion, Environ. Sci. Technol. 46 (2016) 3001–3007.
[3] R.A. Rahman, P. Mehrani, D.Y. Lu, E.J. Anthony, A. Macchi, Investigating the Use of CaO/CuO Sorbents for in Situ CO 2 Capture in a Biomass Gasifier, Energy Fuels 29 (2015) 1504–1510.
[4] Z. Li, Y. Liu, N. Cai, Understanding the effect of inert support on the reactivity stabilization for synthetic calcium based sorbents, Chem. Eng. Sci. 89 (2013) 235–243.
[5] B. Feng, H. An, W. Tan, Screening of CO_2 adsorbing materials for zero emission power generation systems, Energy Fuels 21 (2007) 426–434.
[6] J. Abanades, R. Murillo, J.R. Fernandez, G. Grasa, I. Martínez, New CO_2 capture process for hydrogen production combining Ca and Cu chemical loops, Environ. Sci. Technol. 44 (2010) 6901–6904.
[7] W. Liu, F. Bo, Y. Wu, G. Wang, J. Barry, J. Da Costa, Synthesis of sintering-resistant sorbents for CO_2 capture, Environ. Sci. Technol. 44 (2010) 3093–3097.
[8] X. Yang, W. Liu, J. Sun, Y. Hu, W. Wang, H. Chen, Y. Zhang, X. Li, M. Xu, Preparation of Novel Li_4SiO_4 Sorbents with Superior Performance at Low CO_2 Concentration, Chemsuschem 9 (2016) 1607–1613.
[9] X. Yang, W. Liu, J. Sun, Y. Hu, W. Wang, H. Chen, Y. Zhang, X. Li, M. Xu, Alkali-Doped Lithium Orthosilicate Sorbents for Carbon Dioxide Capture, Chemsuschem 9 (2016) 2480–2487.
[10] A.M. Kierzkowska, P. Roberta, C.R. Müller, CaO-Based CO_2 Sorbents: From Fundamentals to the Development of New, Highly Effective Materials, Chemsuschem 6 (2013) 1130–1148.
[11] R.K. Lyon, J.A. Cole, Unmixed combustion: an alternative to fire, Combust. Flame 121 (2012) 249–261.
[12] I. Martínez, M.C. Romano, J.R. Fernández, P. Chiesa, R. Murillo, J.C. Abanades, Process design of a hydrogen production plant from natural gas with CO_2 capture based on a novel Ca/Cu chemical loop, Appl. Energy 114 (2014) 192–208.
[13] S. Wu, Q. Li, J. Kim, K. Yi, Properties of a Nano CaO/Al_2O_3 CO_2 Sorbent, Ind. Eng. Chem. Res 47 (2008) 180–184.
[14] C. Qin, W. Liu, H. An, J. Yin, B. Feng, Fabrication of CaO-based sorbents for CO_2 capture by a mixing method, Environ. Sci. Technol. 46 (2012) 1932–1939.
[15] V. Manovic, E.J. Anthony, CaO-Based Pellets with Oxygen Carriers and Catalysts, Energy Fuels 25 (2011) 4846–4853.
[16] B. Duhoux, P. Mehrani, D.Y. Lu, R.T. Symonds, E.J. Anthony, A. Macchi, Combined Calcium Looping and Chemical Looping Combustion for Post-Combustion Carbon Dioxide Capture: Process Simulation and Sensitivity Analysis, Energy Technol. 4 (2016) 1158–1170.
[17] D.C. Ozcan, A. Macchi, D.Y. Lu, A.M. Kierzkowska, H. Ahn, C.R. Müller, S. Brandani, Ca–Cu looping process for CO_2 capture from a power plant and its comparison with Ca-looping, oxy-combustion and amine-based CO_2 capture processes, Int. J. Greenh. Gas Con. 43 (2015) 198–212.
[18] M. Vasilije, E.J. Anthony, Integration of calcium and chemical looping combustion using composite CaO/CuO-based materials, Environ. Sci. Technol. 45 (2011) 10750–10756.
[19] A.M. Kierzkowska, C.R. Müller, Sol–Gel-Derived, Calcium-Based, Copper-Functionalised CO_2 Sorbents for an Integrated Chemical Looping Combustion-Calcium Looping CO_2 Capture Process, ChemPlusChem 78 (2013) 92–100.
[20] S.S. Kazi, A. Aranda, L.D. Felice, J. Meyer, R. Murillo, G. Grasa, Development of Cost Effective and High Performance Composite for CO_2 Capture in Ca-Cu Looping Process, Energy Procedia 114 (2017) 211–219.
[21] J. Chen, L. Duan, F. Donat, C.R. Müller, E.J. Anthony, M. Fan, Self-activated, Nanostructured Composite for Improved CaL-CLC technology, Chem. Eng. J. 351 (2018) 1038–1046.
[22] C. Qin, J. Yin, W. Liu, H. An, B. Feng, Behavior of CaO/CuO Based Composite in a Combined Calcium and Copper Chemical Looping Process, Ind. Eng. Chem. Res. 51 (2012) 12274–12281.
[23] F.N. Ridha, D. Lu, A. Macchi, R.W. Hughes, Combined calcium looping and chemical looping combustion cycles with CaO–CuO pellets in a fixed bed reactor, Fuel 153 (2015) 202–209.
[24] A.M. Kierzkowska, C.R. Müller, Development of calcium-based, copper-functionalised CO_2 sorbents to integrate chemical looping combustion into calcium looping, Energy Environ. Sci. 5 (3) (2012) 6061–6065.
[25] C. Qin, J. Yin, C. Luo, H. An, W. Liu, B. Feng, Enhancing the performance of CaO/CuO based composite for CO_2 capture in a combined Ca–Cu chemical looping process, Chem. Eng. J. 228 (2013) 75–86.
[26] V. Manovic, E.J. Anthony, Carbonation of CaO-Based Sorbents Enhanced by Steam Addition, Ind. Eng. Chem. Res. 49 (2014) 9105–9110.
[27] V. Manovic, Y. Wu, I. He, E.J. Anthony, Core-in-shell CaO/CuO-based composite for CO_2 capture, Ind. Eng. Chem. Res. 50 (2011) 12384–12391.
[28] C. Qin, Fuel 181 (2015) 522–530.
[29] W. Peng, Z. Xu, C. Luo, H. Zhao, Tailor-Made Core-Shell CaO/TiO_2–Al_2O_3 Architecture as a High-Capacity and Long-Life CO_2 Sorbent, Environ. Sci. Technol. 49 (2015) 8237–8245.
[30] W. Peng, Z. Xu, H. Zhao, Batch fluidized bed test of SATS-derived CaO/TiO_2 –Al_2O_3 sorbent for calcium looping, Fuel 170 (2016) 226–234.
[31] D. Mei, H. Zhao, S. Yan, Kinetics model for the reduction of Fe_2O_3/Al_2O_3 by CO in Chemical Looping Combustion, Chem. Eng. Process. Process Intensification 124 (2018) 137–146.
[32] L. Guo, H. Zhao, K. Wang, D. Mei, Z. Ma, C. Zheng, Reduction kinetics analysis of sol–gel-derived CuO/$CuAl_2O_4$ oxygen carrier for chemical looping with oxygen uncoupling, J. Therm. Anal. Calorim. 123 (2016) 745–756.
[33] D. Mei, A. Abad, H. Zhao, J. Adánez, Characterization of a sol–gel derived CuO/$CuAl_2O_4$ oxygen carrier for chemical looping combustion (CLC) of gaseous fuels: relevance of gas–solid and oxygen uncoupling reactions, Fuel Process. Technol. 133 (2015) 210–219.
[34] D. Mei, H. Zhao, Z. Ma, C. Zheng, Using the Sol – Gel-Derived CuO/$CuAl_2O_4$ Oxygen Carrier in Chemical Looping with Oxygen Uncoupling for Three Typical Coals, Energy Fuels 27 (2013) 2723–2731.
[35] A. Shulman, E. Cleverstam, T. Mattisson, A. Lyngfelt, Manganese/Iron, Manganese/Nickel, and Manganese/Silicon Oxides Used in Chemical-Looping With Oxygen Uncoupling (CLOU) for Combustion of Methane, Energy Fuels 23 (2009) 5269–5275.
[36] Z. Li, F. Fang, X. Tang, N. Cai, Effect of Temperature on the Carbonation Reaction of CaO with CO_2, J. Occup. Organ. Psych. 68 (2012) 321–326.
[37] J. Fernández, J. Abanades, Overview of the Ca–Cu looping process for hydrogen production and/or power generation, Curr. Opin. Chem. Eng. 17 (2017) 1–8.
[38] L. Diego, F. GarcíA-Labiano, J. Adánez, P. Gayán, A. Abad, B.M. Corbella, J.M. Palacios, Development of Cu-based oxygen carriers for chemical-looping combustion, Fuel 83 (2004) 1749–1757.